Influence of Sr on the formation of Fe-rich phases in Al-10wt% Si casting alloys

M. Timpel[a,*], N. Wanderka[a], R. Grothausmann[a], J. Banhart[a,b]

[a] *Helmholtz-Zentrum Berlin für Materialien und Energie GmbH, Hahn-Meitner-Platz 1, D-14109 Berlin, Germany*
[b] *Technische Universität Berlin, Werkstoffwissenschaften und -Technologien, Hardenbergstr. 36, 10623 Berlin, Germany*

Abstract

The addition of Sr to Al-Si-based alloys is known to modify the morphology of eutectic Si and influences the size of eutectic grains. Knowledge of the distribution and morphology of constituent phases in the eutectic grains such as Fe-rich intermetallic phases can yield an insight into the eutectic grain structure formed during solidification. The effect of Sr addition to an Al-10Si alloy and its influence on the formation of Fe-rich phases was studied by comparison with unmodified eutectic grain structure. The analysis with transmission electron microscopy revealed existance of two types of Fe-rich phases (α-$Al_{14}Fe_3Si_2$ and δ-Al_4FeSi_2) in Sr-modified Al-10Si alloy and only small-scale Fe-rich α-phases in the unmodified alloy. The three-dimensional morphology of eutectic Si and Fe-rich phases was investigated with focused ion beam tomography. The Fe-rich α-phase was found to form in concentrated networks of sheet-shaped inclusions whereas the Fe-rich δ-phase exists as thin platelets. The evolution of eutectic grains and locations of Fe-rich

*Corresponding author
Email address: melanie.timpel@helmholtz-berlin.de (M. Timpel)

phases within the eutectic grain structure are described in detail.

Keywords:
FIB tomography, Al-Si alloys, Sr modification, Fe-rich phases, Eutectic solidification

1. Introduction

Treatment of Al-Si melts through the addition of microstructure-modifying elements such as Na or Sr is common practice to improve mechanical properties of Al-Si casting components [1]. In the past few decades, many researchers have investigated the effect of modifiers on the Al-Si eutectic microstructure, especially the influence on eutectic nucleation and growth. The most striking feature of eutectic modification is the transition of Si morphology from coarse interconnected plates to fine fibrous and coral-like networks [2, 3]. In addition, it has been observed that a transition of the Si morphology from fibrous to plate-like and back to fibrous can occur during growth of an individual eutectic grain [4, 5]. Several studies showed that nucleation of eutectic Si also plays an important role in modification [5–9]. The addition of modifiers considerably decreases the eutectic grain density leading to an increased size of eutectic grains by at least one order of magnitude [5]. This effect is attributed to a strong interaction of Sr with potent heterogenous nucleation sites for Si [6, 7, 9].

Beside eutectic modification, evolution of eutectic grain structure is critically influenced by additional alloying and/or impurity elements. For instance, commercial Al-Si based alloys always contain certain amounts of Fe impurities that generally cannot be removed from the melt in a cost efficient way. During solidification, Fe segregates and forms complex intermetallic phases. Several Fe-rich phases such as α-Al_8Fe_2Si or α-$Al_{15}(Fe,Mn)_3Si_2$, β-Al_5FeSi, δ-Al_4FeSi_2 and π-$Al_8Mg_3FeSi_6$ have been identified in Al-Si casting alloys, strongly depending on the composition and cooling conditions of the alloy [10–12]. The formation of brittle Fe-rich phases, which appear as needles/plates in the microstructure, can cause adverse effects on castability and mechanical properties of an alloy [10, 13]. Therefore, understanding the formation and the stability of Fe-rich phases is of considerable technological importance. Fe-rich phases in Na- and Sr-modified Al-Si alloys have been extensively studied [14–20], but the influence of Sr on the formation of Fe-rich phases in Al-Si alloys is still under debate [16, 18, 19].

To understand microstructure formation in three dimensions (3D), the use of tomographic techniques has become indispensable [21–23]. The objective of the present work is to investigate the 3D morphology of Fe-rich phases in Sr-modified Al-10Si containing 0.1 wt% Fe by focused ion beam (FIB) tomography. The eutectic grain morphology was additionally investigated using optical microscopy and scanning electron microscopy (SEM). The structure and composition of Fe-rich phases was identified by transmission electron microscopy (TEM).

2. Experimental

2.1. Alloy preparation

Al-10Si (wt%) alloys were manufactured by Rheinfelden Alloys GmbH (Rheinfelden, Germany). Approximately 9 kg of commercially pure Al and Si were melted at 760°C in an induction furnace. The melt was degassed in

Ar atmosphere for 15 min and additional 5 min in Ar and Cl atmosphere. For modification, an Al-10Sr master alloy was added and the melt was held at 760°C for 20 min to ensure complete dissolution. Chemical analysis was then performed using an optical emission spectrometer. The chemical compositions of both unmodified and Sr-modified Al-10Si alloy are listed in Table 1.

The unmodified and Sr-modified melt were cast into a cylindrical permanent mold (30 mm diameter and 200 mm height). The total solidification time was approximately 30-40 s.

2.2. Microstructural characterization

The cast rods were metallographically prepared as previously described in Ref. [22]. All specimens investigated in the present study were extracted from the centers of the castings about 15 mm from the bottom of the ingot. Samples for optical microscopy were etched for 30 s at 20°C in a mixture of 60 ml water, 10 g sodium hydroxide and 5 g potassium ferricyanide (modified Murakami's reagent) to reveal details of the eutectic grain morphology [24, 25].

For TEM analysis, the samples were prepared by mechanically polishing and Ar ion beam thinning as previously described in Ref. [22]. In order to find the features of interest along electron-transparent regions, the TEM lamella was first inspected in a SEM. The TEM analysis of Fe-rich phases was then carried out using a Philips CM30 microscope operating at 300 kV and equipped with an EDAX Genesis EDX system. The chemical composition of the constituent phases was analyzed by TEM-EDX using a minimum of five measurements for each Fe-rich phase. Crystal structures of the phases were determined by selected area electron diffraction (SAED).

For 3D characterization of the eutectic grains, a Zeiss 1540EsB CrossBeam® workstation was employed. Two distinct locations in an eutectic grain of the Sr-modified alloy were investigated by FIB tomography. FIB serial sectioning was performed using 30 keV Ga ions with an ion beam current of 200 and 1000 pA corresponding to a milling step in z-direction of 20 and 35 nm, respectively. A secondary electron (SE) in-lens detector was used for SEM imaging of 2D slices. Due to the low acceleration voltage used for imaging (2 kV), the SE electrons detected give rise to a signal sensitive to the surface conductivitiy of the material and yields high-resolution images [26].

The software ImageJ with the plugin *stackreg* [27] was used to recursively align the image stacks. A variation in signal intensity of imaged 2D slices is caused by shadowing due to the geometry of the FIB/SEM system [28]. 2D image filters were applied to eliminate shadowing effects, remove background and to enhance contrast between eutectic phases. The 3D micostructure of eutectic Si and Fe-rich phases were visualized using the software VGStudio MAX 2.1, after processing with a 5×5×5 median filter to reduce noise. Application of global thresholds yields segments of each different phase. Volume fractions of the segments corresponding to eutectic Si and Fe-rich phases were determined.

3. Results

3.1. Microstructural features

The typical eutectic microstructure of the alloys as investigated by SEM is shown in Fig. 1a without modifier and (b) with addition of 200 ppm Sr. The unmodified eutectic (Fig. 1a) consists of coarse acicular Si plates (dark gray) embedded in an eutectic Al matrix. Fe-rich phases with so-called "Chinese script" morphology (light gray) are uniformly distributed throughout the eutectic microstructure. They are often located along eutectic Si plates, as marked by arrows in Fig. 1a, and exhibit sizes in the order of 5 μm (measured on sample surface).

The microstructure of the Sr-modified eutectic is illustrated in Fig. 1b. The modified eutectic exhibits the typical fine fibrous Si structure. In addition, the eutectic exhibits a cellular sub-structure with Fe-rich phases of so-called "Chinese script" 2D morphology segregated at the cell boundaries (marked by arrows). At these boundaries the eutectic Si locally exhibits larger fiber spacings than the fine eutectic in the center of the cells. Several Fe-rich phases are also observed adjacent to primary Al dendrites as indicated by the left arrow in Fig. 1b.

The eutectic grain structure and Fe-rich phases were enhanced by etching the surface of the Sr-modified alloy and subsequently imaged in the optical microscope using differential interference contrast, see Fig. 2. Many spherical features appear in light red and are surrounded by darker regions (Fig. 2a). Beside the eutectic microstructure, primary Al dendrites are found uniformly distributed across the sample. The spherical features can be attributed to the center of eutectic grains as previously observed by McDonald et al. [5].

The area marked by a rectangle in Fig. 2a has been investigated in more detail and is magnified in Fig. 2b. Three distinct regions are found there:

- **Region 1**: In the center of the circular features, the eutectic is extremely fine-scale and well-modified and the Si appears completely fibrous. No Fe-rich phases could be observed within this central region.

- **Region 2** is the region surrounding region 1 and appears also bright. The eutectic in this transitional band is well-modified, too, but contains boundaries between eutectic cells, as observed in Fig. 1b. The boundaries are decorated by segregated Fe-rich phases as marked by the white arrow in region 2 of Fig. 2b.

- In **region 3**, the Si fibers exhibit aligned growth, i.e. preferred growth radially from the central region. In addition, thin Fe-rich platelets that are not found in the unmodified eutectic are located in this region, often delineating cell boundaries (marked by white arrows in region 3 of Fig. 2b).

To unambigously identify the type of Fe-rich phases in the Sr-modified eutectic, both structure and composition analysis were carried out in the TEM. A Fe-rich phase with "Chinese script" morphology as found in region 2 is imaged by bright-field TEM (dark gray) in Fig. 3a. The phase grows without developing facets and has a strongly curved and non-convex surface. The corresponding SAED pattern is displayed in Fig. 3b. The structure of these Fe-rich phase was found to be body-centered cubic (bcc), space group Im3, with a lattice parameter a=1.253 nm. From SAED patterns from different areas of the Fe-rich phase segregation in Fig. 3a it was found that the whole phase consists of polycrystallites connected to each other during growth. The average chemical composition of this Fe-rich phase as given in Table 2 indicates a stochiometry of $Al_{14}Fe_3Si_2$.

A bright-field TEM image of Fe-rich platelets (dark gray) is presented in

Fig. 3c. Many twins are observable along the growth direction of the platelets indicating faceted growth of this phase along specific directions. The SAED pattern in Fig. 3d taken from the Fe-rich platelet indicated by the arrow in Fig. 3c corresponds to a tetragonal structure with the unit cell of $PdGa_5$-type and lattice parameters a=0.614 nm, c=0.957 nm. This structure is in accordance with the Al_3FeSi_2-phase observed in Ref. [29] and designated as Fe-rich δ-phase [30]. In the present study, the Fe-rich δ-phase appears with the slightly different stochiometry Al_4FeSi_2. The Fe-rich δ-phase contains a higher Si content than the Fe-rich α-phase (see Table 2).

In order to investigate the eutectic grain structure on the μm scale, site-specific FIB milling and SEM imaging of 2D slices were performed at three distinct locations in the eutectic grain as indicated in Fig. 2b. As displayed in Fig. 4, 2D slices from (a) well-modified fine eutectic (found not only in region 1, but also in the center of eutectic cells in region 2), (b) boundaries with coarser but still modified eutectic and Fe-rich phases with "Chinese script" morphology (found in region 2), and (c) boundaries with fine Si fibers and Fe-rich platelets (found in region 3) are presented. Stacks of 2D images as shown in Fig. 4b and (c) are further used for 3D visualization of the Fe-rich phases and the adjacent Si eutectic, see chapter 3.2. Gray level variations observed in the Al matrix in Fig. 4 are attributed to channeling contrast. The different gray levels in the Al matrix thus correspond to slightly different crystallographic orientations of individual eutectic Al grains.

The fine eutectic in Fig. 4a consists of very fine Si fibers, which appear as round particles in 2D, with fine fiber spacing in the order of 1 μm and an eutectic Al matrix with no notable variations in crystallographic orientation.

This indicates continuous growth of Al in the fine eutectic regions. At the boundary of the eutectic cells in region 2 (Fig. 4b) the Fe-rich α-phase with typical "Chinese script" morphology (white) is observed. At this boundaries, Si fibers are coarser and less rounded with larger spacing in the order of 2 μm. The eutectic Al exhibits boundaries from different Al grains that have impinged on each other (marked by arrows). At the interface of the Al grains the Fe-rich α-phase is segregated as inclusion. It is observed that the size of the Fe-rich α-phases in the Sr-modified alloy are larger than that in the unmodified eutectic, i.e. sizes > 5 μm.

The eutectic at the cell boundaries in region 3 (Fig. 4b) exhibits fine Si fibers with slightly different growth directions at both sides of the polycrystalline Al matrix. Close to the boundaries of the Al grains (marked by arrows) thin Fe-rich δ-platelets (white) are located. These are not observed directly at the interfaces of the Al grains. The Fe-rich δ-platelets can be up to a few μm long (as measured on sample surfaces). They grow anisotropically and are extremely thin ($\leq$ 250 nm) with respect to their other two dimensions. Furthermore, in the present study, we observed that Fe-rich δ-platelets which appear isolated in two dimensions are often interconnected in 3D.

3.2. FIB tomography

The 3D microstructure of eutectic Si and Fe-rich α-phase at the cell boundary of the eutectic in region 2 is illustrated in Fig. 5a. FIB serial sectioning was performed along the boundary marked by the arrow in region 2 of Fig. 2b so that the z-axis of the visualized volumes is oriented along the cell boundary. The eutectic Si at the cell boundary does not appear fine and fibrous, but as a mixed structure of thin Si platelets and less rounded fibrous Si, indicating a gradual transition of the structure from fine fibers into coarse Si plates. This coarse and intermixed Si structure is less branched than the fine Si fibers in the center of the cells. It is observed that the Fe-rich α-phase is precipitated as inclusion at the impingment of two eutectic cells. Figure 5a reveals the 3D shape of the Fe-rich α-phase as thin sheets segregated in an concentrated network.

A separate 3D visualization of the Fe-rich α-phase from a different perspective is shown in Fig. 5b. In 3D, the true shape of the Fe-rich α-phase no more resembles a "Chinese script" but appears with a very complex and non-convex surface reflecting imprints of the surrounding eutectic. Furthermore, it is obvious that the Fe-rich α-phase consists of several phases that have segregated at the eutectic boundaries. The estimated volume fractions of eutectic Si and Fe-rich α-phase in an investigated volume of $20.6\times14.3\times11.2\ \mu m^3$ are 14.9 vol% and 2.24 vol%, respectively.

In Fig. 6a, the 3D microstructure of the Si fibers and Fe-rich δ-platelets at a typical cell boundary in region 3 is displayed. A preferred orientation of the Si fibers towards the Fe-rich δ-platelets is clearly visible. Several morphological features are observed on the surfaces of the Fe-rich δ-platelets, see Fig. 6b. The development of holes in the Fe-rich δ-platelets corresponds to their growth around Si fibers. The lateral growth and thus increase of the thickness of Fe-rich δ-platelets can result in imprints of the surrounding Si fibers being formed on the surface of Fe-rich δ-platelets. The estimated volume fractions of eutectic Si and Fe-rich δ-phase in an investigated volume of $10.2\times6.4\times5.0\ \mu m^3$ are 18.8 vol% and 1.98 vol%, respectively.

4. Discussion

The microstructure of the unmodified eutectic in Fig. 1a clearly indicates an uniform distribution of the cubic Fe-rich α-phase across the eutectic grains. In 3D, the unmodified eutectic Si forms a highly interconnected and plate-like network [3, 22]. The development of 3D morphology of the Fe-rich α-phase in the unmodified Al-Si alloy has been described by a model proposed in our previous work [22]. The model assumes that the Fe-rich α-phase develops as inclusion in small liquid pockets that get isolated between the unmodified Si plates protruding ahead of the polycristalline Al matrix. Due to the branching of the Si plates (irregular eutectic) and the relatively high number of eutectic nucleation events, the isolated pockets are uniformly distributed throughout the unmodified eutectic grains.

Addition of Sr to the Al-Si alloy refines the eutectic Si from an interconnected plate-like network (Fig. 1a) into a fine fibrous morphology (Fig. 1b). In accordance to previous results [5, 25] large eutectic grains with radii >1000 μm were observed in the present work. Furthermore, the eutectic grains exhibit cellular sub-structures as previously reported in Ref. [31] with Fe-rich phases at eutectic cell boundaries. In the present study, three regions with different microstructural features can be assigned within the modified eutectic microstructure of an individual grain:

- **Region 1**: Center of the grain that is free of eutectic cell boundaries and Fe-rich phases
- **Region 2**: Transitional region with cellular sub-structure and Fe-rich α-phases of 2D "Chinese script" morphology along eutectic cell bound-

aries

- **Region 3**: External regions with preferred growth direction of the eutectic Si and Fe-rich δ-platelets in interconnected networks along eutectic cell boundaries

According to McDonald et al. [5], three distinct regions with changes of Si morphology are related to the variation of the velocity of the solid-liquid (s-l) interface during eutectic solidification. In contrast to this previous work, less variation in Si morphology is observed in the present study, i.e. no transition to plate-like and back to fibrous morphology could be observed. This is due to the much higher cooling rate of the permanent mold cast alloys investigated here. The more rapid rate of heat extraction in the permanent mold limits the amount of recalescence and grain growth follows a more or less accelerating interface throughout the entire eutectic solidification.

The Fe-rich α-phase with cubic crystal structure (bcc, a=1.253 nm) and a stochiometry of ($Al_{14}Fe_3Si_2$) in the Sr-modified Al-10Si alloy is very similar to that found in the unmodified alloy. However, the Fe-rich α-phase in the Sr-modified alloy was found to be more inhomogenously distributed and exhibits coarser morphology than in the unmodfied alloy.

The second type of Fe-rich phase, namely the metastable δ-Al_4FeSi_2 phase with tetragonal crystal structure (Fig. 3b), thin platelet morphology (Fig. 6b) and nearly equal fraction of Fe and Si (see Table 2) is only found in the Sr-modified alloy. These fine Fe-rich δ-platelets have previously been observed in Sr-modified Al-11Si [32] and Al-15Si [22] alloys.

Several studies have mentioned about thin β-Al_5FeSi platelets in both Na-modified [6, 33] and Sr-modified Al-Si alloys [5, 16, 20]. The identification of such Fe-rich phases has only been based on their morphology and/or EDX analysis but not on their structure determination. However, the Fe-rich monoclinic β-phase with Fe/Si ratio of about 2 was not found in the alloys investigated. Fe-rich phases with platelet morphology are often misleadingly identified as Fe-rich β-phase in Al-Si alloys as reported in Ref. [34]. Therefore, it can not be ruled out that the thin Fe-rich platelets observed in previous studies [5, 6, 16, 20, 33] in fact correspond to the Fe-rich δ-phase.

Due to the comprehensive studies at different length scales, we are able to assign the locations of both Fe-rich phases to the morphological evolution of the eutectic growth front during grain growth. In the following, the formation of both Fe-rich phases with respect to their locations in the eutectic grain is qualitatively explained on the basis of the morphological evolution of the eutectic growth front with addition of Sr and its influence on Fe segregation in the Al-Si melt.

4.1. Region 1: Center of the grain

In the initial stages of eutectic solidification a roughly spherical and coupled growth front of the eutectic phases can be assumed [35]. The fine and well-modified eutectic consists of fine Si fibers growing as a coral-like network of Si-skeletons embedded in an eutectic Al matrix and is free of Fe-rich phases (see Fig. 4a). The eutectic Al matrix forms a coupled growth front with the coral-like Si-skeletons (regular eutectic) and does not grow in form of polycristalline sub-grains. Therefore, the eutectic Al exhibits no interfaces with segregated Fe-rich phases in the well-modified central region 1.

4.2. Region 2: Transition region

During grain growth, the roughly spherical eutectic growth front may build up a solute layer of impurity elements ahead of the solid-liquid (s-l) interface leading to a constitutional undercooling at the growth front [36]. Figure 7a schematically illustrates the morphological evolution of the eutectic growth front and the suggested locations of crystallization of Fe-rich α-phase (see magenta-colored arrows in Fig. 7a) during grain growth in the transition region 2. Primary Al dendrites are not shown here for clarity.

As illustrated in Fig. 7a, the enrichment of impurities (in addition to the decrease of growth velocity due to recalescence) induces a gradual breakdown of the coupled growth front into individual cells in region 2. The local reduction of the enriched layer due to the formation of isolated liquid pockets in the eutectic grain effectively reduces the amount of constitutional undercooling at the eutectic growth front. It forms an eutectic mushy zone [36] with the fine eutectic in the center of the cells and coarser eutectic as well as Fe-rich α-phases at the boundaries (see Fig. 1b). Furthermore, the breakdown of the coupled growth front and accumulation of impurity elements may preferentially occur at sites of perturbations during growth, e.g. when the grain impinges on "‘obstacles"’ such as primary Al dendrites. Therefore, Fe-rich phase segregation from the surrounding solid is likely to occur next to pre-existing Al dendrites as observed in Fig. 1b.

Due to the recalescence at the minimum in the cooling curve, the growth of the eutectic grains in the melt is continually slowed down [5]. Solute redistribution calculations [37] suggest that for an accelerating growth front the concentration of elements in the solute layer is continually increasing, whereas the concentration is continually decreasing when the grwoth front is decelerated. Therefore, the breakdown of the coupled growth front in region 2 is additionally favoured by the decreasing concentration of the modifier Sr at the s-l interface of the growth front during decelerated grain growth and before adjacent grains impinge.

The microscopically visible transition morphology of the eutectic grains with cellular sub-structure was previously described in Ref. [38] as "cauliflower-shaped" morphology of the eutectic grains. The eutectic growth front in region 2, however, is still roughly spherical and the internal fraction of liquid within region 2 relatively low so that most of the Fe impurities still segregates ahead of the eutectic growth front.

4.3. Region 3

In region 3, the eutectic consists of aligned branches radially extending from the spherical center as visible in Fig. 2b. In this stage, the eutectic grain morphology transforms completely into a cellular eutectic and develops strongly pronounced depressions, as schematically illustrated in Fig. 7b. The evolution of interface pertubations of the initially spherical and coupled s-l interface of eutectic grains were recently observed in 3D during directional solidification of an Al-9Si-15Cu alloy modified by 150 ppm Sr [23]. This supports our interpretation of the microstructure in region 3. The eutectic microstructure consists in region 3 of eutectic cells with separated coral-like Si-skeletons that grow radially from the center (see Fig. 2b) with slightly different orientations of the cells (i.e. different fiber spacing). Within the eutectic cells there is still coupled growth of Si fibers with the Al matrix.

The transition from fine eutectic with spherical front to cellular eutectic in the Sr-modified Al-10Si alloy is attributed to a destabilization of the eutectic interface due to the segregation of impurity elements. Similar suggestions to explain the morphological transition from spherical to cellular growth front have been made in binary Sn-Cu solder alloys [39].

It can be concluded that the outwardly directed growth of the coral-like Si-skeletons and the evolution of eutectic cells occurs due to an anisotropy of the interfacial energy $\gamma_{\text{S-l}}$, most likely induced by impurity elements in combination with the increase of growth velocity of the grains during late stages of solidification.

Since the thin Fe-rich δ-platelets are mainly observed at boundaries in region 3 of the eutectic grains, it can be assumed that Fe-rich δ-nucleation occurrs simultaneously during the final stages of Al-Si eutectic reaction. Fe-rich δ-platelets are likely to have formed after severe enrichment of Fe in a Si-rich melt during a second wave of nucleation subject to the availability of suitable nucleants that become activated at higher undercooling [25]. This second wave of nucleation corresponding to second maximum in the undercooling has been previously observed in lamellar graphite cast iron and has been termed "secondary nucleation" [40, 41]. Two suggested locations of crystallization of Fe-rich δ-platelets are marked by the magenta-colored arrows in Fig. 7b.

4.4. Microstructure of the eutectic grain

Fig. 7c schematically shows the solidifed eutectic microstructure in the Sr-modified Al-10Si alloy and the location of the Fe-rich phases in region 2 and 3 of the eutectic grain. In the following, the formation of the two Fe-rich phases with respect to their 3D morphology and growth kinetics is discussed.

4.4.1. Formation of Fe-rich α-phase

The Fe-rich α-phase was found in networks of branched sheets (Fig. 5) mainly in the transition region 2 at the boundaries of eutectic cells. The Fe-rich α-phase is schematically shown in Fig. 7c with its "Chinese script" 2D morphology (magenta-colored in region 2). The 3D morphology is very complex and deviates considerably from a convex shape (see Fig. 5). The Fe-rich δ-phases exhibit the 3D shape of thin sheet-shaped inclusions with strongly curved surfaces. Their sheet-shaped morphology is similar to that in the unmodified alloy. Therefore, it can be assumed that they are formed by the mechanism described in [22], i.e. during late stages of solidification in isolated liquid pockets that are enriched in Fe. However, these isolated liquid pockets are not as finely distributed as in the unmodified eutectic grains, but exist as liquid channels with increased sizes in the eutectic mushy zone of region 2.

During further eutectic growth, Fe is rejected from each growing eutectic cell and accumulates in the liquid channels between the cells. At late stages of solidification, the Fe-rich α-phase finally solidifies as interconnected thin "sheet-shaped" inclusion in concentrated networks along eutectic cell boundaries as observed in Fig. 1b and region 2 of Fig. 2b. It can be concluded that the Fe-rich α-sheets mark the impingement of two separately grown coral-like Si-skeletons represented by the impingement of their polycrystalline Al grains, see Fig. 4b.

At the boundaries in region 2, the eutectic Si appears coarser, less spherical and less branched (Fig. 4b), most likely due to the lack of Sr during final impingement of the eutectic cell resulting in incomplete modification of the

Si morphology.

4.4.2. Formation of Fe-rich δ-platelets

The Fe-rich δ-platelets (see Fig. 6) are located at interconnected networks along eutectic cell boundaries in the external region 3 of the grains. Assuming that these platelets precipite during secondary nucleation events, this will occur during the higher undercoolings at the end of solidifcation. Beside nucleation the stability of phases formed depends on local cooling conditions.

Formation of Fe-rich β-phase is generally favored by low cooling rates [12], whereas the formation of Fe-rich δ-platelets is strongly promoted by high cooling rates, i.e. high undercooling [42]. Considering the Gibbs free energies for the formation of both the Fe-rich β-phase (25 wt% Fe and 12 wt% Si [43]) and the Fe-rich δ-phase (27 wt% Fe und 24.5 wt% Si, see Table 2) using enthalpies of mixing of binary systems provided by Ref. [44] and temperatures below the minimum in the cooling curve (beginning of secondary nucleation, e.g. below 570°C), the calculated Gibbs free energy of Fe-rich δ-phase (-15 kJ/mol) is more negative than that of the Fe-rich β-phase (-12 kJ/mol). This is a plausible explanation for the preferred formation of the Fe-rich δ-phase. Thus, after severe enrichment of Fe and as the rate of cooling increases in the final stages of solidification, Fe-rich δ-platelets precipitate in the remaining melt.

It has been reported that primary Fe-rich β-plates that form prior to the eutectic reaction act as potent nucleation sites for eutectic Si [17, 45]. In the present work it cannot be confirmed that Fe-rich δ-platelets are active nucleants for eutectic grains. However, the formation of fiber imprints on the surfaces of the Fe-rich δ-platelets (see Fig. 6b) can only be explained when the lateral growth of the thickness of Fe-rich platelets follows the surface of already existing Si fibers. In addition, the formation of holes and the growth around Si fibers as observed in Fig. 6a supports that Si fibers exists prior to the growth of Fe-rich δ-platelets.

Not being able to nucleate new eutectic grains, the Fe-rich δ-platelets are engulfed by the impinging branches of cellular eutectic and hence are pushed to the cell and grain boundaries at the end of solidification. The "branching" occurence of Fe-rich δ-platelets appears to be dictated by later impingement of different platelets and may not be crystallographically related (e.g. twinning). The growth kinetics of the highly faceted Fe-rich δ-platelets is anisotropic and it can be assumed that growth of Fe-rich δ-platelets is dictated by the anisotropy of the s-l interfacial energy of the eutectic growth front in the late stages of solidification.

When eutectic solidification is completed, the eutectic grains exhibit a cellular sub-structure with inclusions of Fe-rich α-phases at boundaries in transition region 2 and Fe-rich δ-platelets along eutectic cell boundaries in the external region 3, see Fig. 7c. Furthermore, at impingement of eutectic grains Fe-rich phases are also trapped at the grain boundaries. The cellular sub-structures of the eutectic grains could be observed since the eutectic microstructure of grains approximately sectioned through their center were investigated. In 2D sections of unetched samples the sub-structures are hardly visible and are often superimposed by other truncated grains.

5. Summary

By comparing unmodified and Sr-modified (200 ppm) Al-10Si alloys we found:

- Three regions of eutectic grains in Sr-modified alloy occur: (1) a roughly spherical central region with fine eutectic consisting of fine Si fibers with coupled growth of Al and Si and no Fe-rich phases; (2) a transition region around the central region with departure from spherical growth and Fe-rich α-phase in concentrated networks along the eutectic cell boundaries; (3) external regions with the evolution of a cellular eutectic and thin Fe-rich platelets (δ-phase) at the eutectic cell boundaries

- The small-scale Fe-rich α-phase uniformly distributed was found to form in the unmodified alloy whereas larger Fe-rich α-phases were found in the Sr-modified alloy due to enhanced Fe segregation at the coupled growth front;

- The mechanism of formation of Fe-rich α-phases in both Sr-modified and unmodified alloy seems to be the same due to similar 3D morphology of the phases;

- the formation of metastable Fe-rich δ-platelets in external regions of eutectic grains was found in the modified alloy only;

- the distribution of Fe-rich phases in eutectic grains of the Sr-modified alloy and the evolution of a cell-like sub-structure can be qualitatively explained by the morphological evolution of the s-l interface during growth of eutectic grains.

Acknowledgments

The authors would like to thank Mrs. C. Förster for preparing the TEM samples.

References

[1] Sigworth GK. Int J Metalcast 2008;2:19–41.

[2] Mondolfo LF. J Aust Inst Met 1965;10:169–77.

[3] Lasagni F, Lasagni A, Marks E, Holzapfel C, Mücklich F, Degischer HP. Acta Mater 2007;55:3875–82.

[4] Chen XG, Engler S. Giesserei 1990;77:149–55.

[5] McDonald SD, Dahle AK, Taylor JA, StJohn DH. Metall Mater Trans A 2004;35A:1829–37.

[6] Crosley PB, Mondolfo LF. AFS Trans 1966;74:53–64.

[7] Nogita K, McDonald SD, Tsujimoto K, Yasuda K, Dahle AK. J Electron Microsc 2004;53:361–9.

[8] McDonald SD, Nogita K, Dahle AK. Acta Mater 2004;52:4273–80.

[9] Cho YH, Lee HC, Oh KH, Dahle AK. Metall Mater Trans A 2008;39A:2435–48.

[10] Couture A. Int Cast Met J 1981;6:9–17.

[11] Bäckerud L, Chai G, Tamminen J. Solidifcation Characteristics of Aluminum Alloys; vol. 2. Stockholm: AFS/Skanaluminium; 1990.

[12] Khalifa W, Samuel FH, Gruzleski JE. Metall Mater Trans A 2003;34:807–25.

[13] Taylor JA, Schaffer GB, StJohn DH. Metall Mater Trans A 1999;30:1643–50.

[14] Shabestari SG, Gruzleski JE. AFS Trans 1995;26:285–93.

[15] Mulazimoglu MH, Tenekedjiev N, Closset B, Gruzleski JE. Cast Metals 1993;6:16–28.

[16] Samuel FH, Samuel AM, Doty HW, Valtierra S. Metall Mater Trans A 2001;32:2061–75.

[17] Shankar S, Riddle YW, Makhlouf MM. Acta Mater 2004;52:4447–60.

[18] Lu L, Dahle AK. Metall Mater Trans A 2005;36A:819–35.

[19] Khalifa W, Samuel A, Samuel F, Doty H, Valtierra S. Int J Cast Metal Res 2006;19:156–66.

[20] Suarez-Pena B, Asensio-Lozano J. Scripta Mater 2006;54:1543–8.

[21] Terzi S, Taylor JA, Cho YH, Salvo L, Suery M, Boller E, et al. Acta Materialia 2010;58:5370–80.

[22] Timpel M, Wanderka N, Murty BS, Banhart J. Acta Mater 2010;58:6600–8.

[23] Mathiesen RH, Arnberg L, Li Y, Meier V, Schaffer PL, Snigireva I, et al. Metallurgical and Materials Transactions A-Physical Metallurgy and Materials Science 2011;42A:170–80.

[24] Petzow G. Metallographisches, keramographisches und plastographisches Ätzen. Berlin Stuttgart; 1994.

[25] McDonald S. Eutectic solidification and porosity formation in unmodified and modified hypoeutectic aluminium-silicon alloys. Ph.D. thesis; 2002.

[26] Reimer L. Scanning electron microscopy: physics of image formation and microanalysis. Springer, Berlin; 1998.

[27] Thevenaz P, Ruttimann UE, Unser M. IEEE Trans Image Process 1998;7:27–41.

[28] Holzer L, Indutnyi F, Gasser PH, Münch B, Wegmann M. J Microsc-Oxford 2004;216:84–95.

[29] Gueneau C, Servant C, Dyvoire F, Rodier N. Acta Cryst C 1995;51:177–9.

[30] Mondolfo LF. Aluminum alloys: structure and properties. London: Butterworth; 1976.

[31] Chen XG. Kristallisation des aluminium-silicium-eutektikums und anwendung der thermischen analyse zur kontrolle der veredelung. Ph.D. thesis; 1990.

[32] Kral MV, Nakashima PNH, Mitchell DRG. Metall Mater Trans A 2006;37A:1987–97.

[33] Powell GLF, Colligan GA. Materials Research Bulletin 1970;5:431–6.

[34] Kral MV. Mater Lett 2005;59:2271–6.

[35] Dinnis CM, Dahle AK, Taylor JA. Mat Sci Eng A 2005;392:440–8.

[36] Heiberg G, Nogita K, Dahle AK, Arnberg L. Acta Mater 2002;50:2537–46.

[37] Smith VG, Tiller WA, Rutter JW. Canadian Journal of Physics 1955;33:723–45.

[38] Chen XG, Ellerbrok R, Engler S. Giessereiforschung 1990;42:1–10.

[39] Ventura T, Terzi S, Rappaz M, Dahle AK. Acta Materialia 2011;59:1651–8.

[40] Fras E, Kapturkiewicz W, Burbielko A, Lopez H. AFS Trans 1996;96:1–4.

[41] Kapturkiewicz W, Fras E, Burbelko AA. Archives of Metallurgy and Materials 2009;54:369–80.

[42] Khalifa W, Samuel FH, Gruzleski JE, Doty HW, Valtierra S. Metall Mater Trans A 2005;36A:1017–32.

[43] Belov N, Eskin D, Aksenov A. Multicomponent Phase Diagrams: Applications for Commercial Aluminum Alloys. Elsevier; 2005.

[44] Takeuchi A, Inoue A. Materials Transactions 2005;46:2817–29.

[45] Liu L, Samuel AM, Samuel FH, Doty HW, Valtierra S. International Journal of Cast Metals Research 2003;16:397–408.

Tables

Table 1: **Chemical composition of the unmodified and Sr-modified Al-10Si alloy with main elements Al, Si, Fe (in wt%) and additional impurity levels (in ppm).**

Alloy	Al	Si	Fe	Cu	Mn	Mg	Cr	Ti	Ni	Ga	V	P	Sr
	wt%			ppm									
Unmodified	89.8	10.1	0.1	10	20	10	11	61	38	41	102	3	<1
Sr-modified	89.8	10.0	0.1	10	20	10	11	60	38	42	102	4	201

Table 2: **Crystal structure and average composition of Fe-rich phase (in at%) in the eutetic grains as measured by selected area electron diffraction and energy dispersive spectroscopy, respectively, in the transmission electron microscope. The morphology of Fe-rich phase known as "Chinese script" in 2D corresponds to the thin sheet-shaped morphology observed in 3D. The Fe/Si ratio was calculated from wt% for comparison with literature data.**

Fe-rich phase	3D Morphology	Crystal structure	Lattice parameters	Al	Si	Fe	Fe/Si
			nm	at%			
α	Branched sheets	Cubic (bcc)	a=1.253	73.6	10.4	16.0	3.1
δ	Platelets	Tetragonal	a=0.614; c=0.957	57.1	27.6	15.3	1.1

Figures

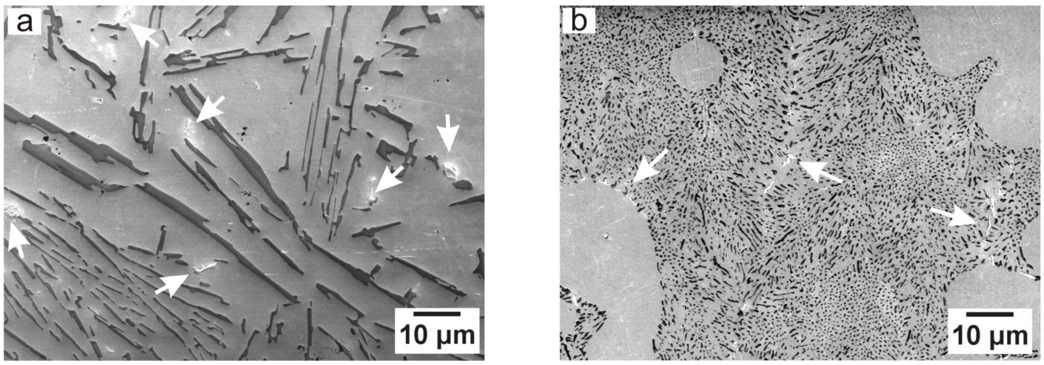

Figure 1: SEM images showing the microstructure of (a) unmodified and (b) Sr-modified Al-10Si alloy. Fe-rich phases in both alloys are marked by arrows.

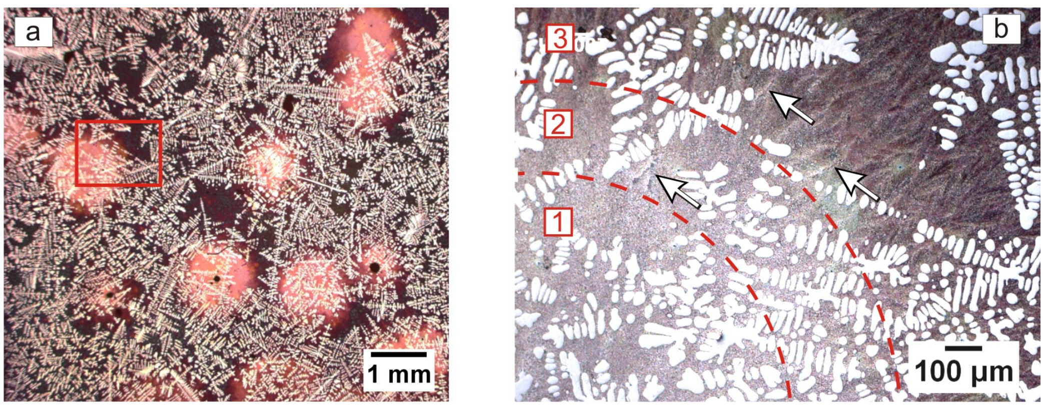

Figure 2: Optical micrographs taken from the etched surface of the Sr-modified Al-10Si alloy obtained using differential interference contrast. (a) Light red areas are central regions of eutectic grains and dark areas are external regions. The area marked by the rectangle is magnified in (b). Three regions with different microstructural features of an eutectic grain are labelled: central region 1 that contains no Fe-rich phases; region 2 exhibiting transitional cell-like structure with Fe-rich phases at cell boundaries (marked by arrow); region 3 exhibiting modified eutectic with aligned Si growth and Fe-rich platelets at cell boundaries (marked by arrow).

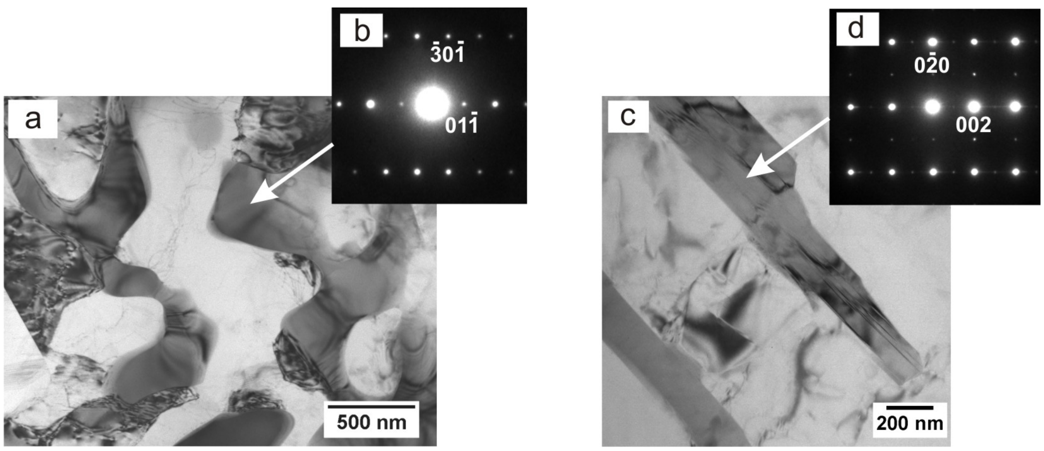

Figure 3: Bright-field TEM images of microstructural features obtained from different locations in the eutectic grain of the Sr-modified Al-10Si alloy: (a) Fe-rich α-phase with "Chinese script" morphology (dark gray) as observed in region 2 of Fig. 2(b); (b) SAED pattern of the Fe-rich α-phase along the $[\bar{1}33]$ zone axis; (c) Fe-rich δ-phase with platelet morphology (dark gray) as observed in region 3 of Fig. 2(b); (d) SAED pattern obtained from the Fe-rich δ-platelet along the [100] zone axis.

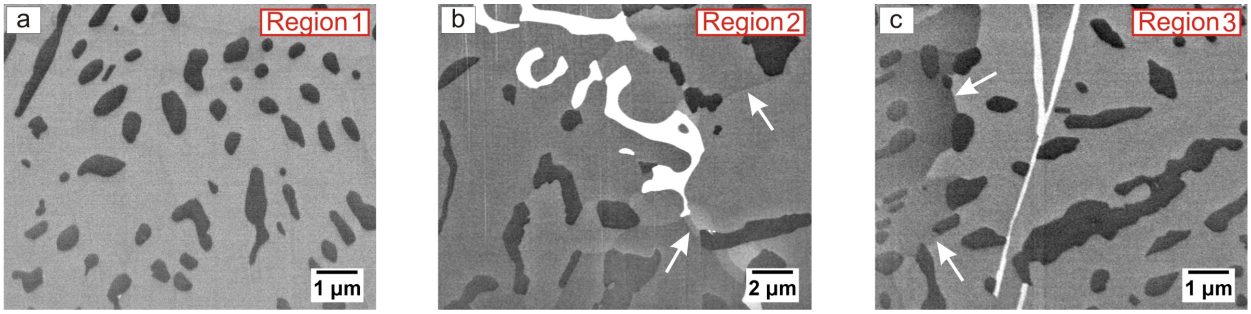

Figure 4: Microstructural features observed at different locations in the eutectic grain of the Sr-modified Al-10Si alloy imaged by SE (in-lens) detector in SEM: (a) very fine eutectic containing fibrous Si (dark) belongs to the region 1 of Fig. 2(b), no Fe-rich phases are visible; (b) coarse eutectic containing Fe-rich α-phase with "Chinese script" morphology (white) found at boundaries in region 2 of Fig. 2(b); (c) eutectic with aligned Si growth containing Fe-rich δ-platelets found at boundaries in region 3 of Fig. 2(b). The arrows indicate interfaces between individual grains of eutectic Al.

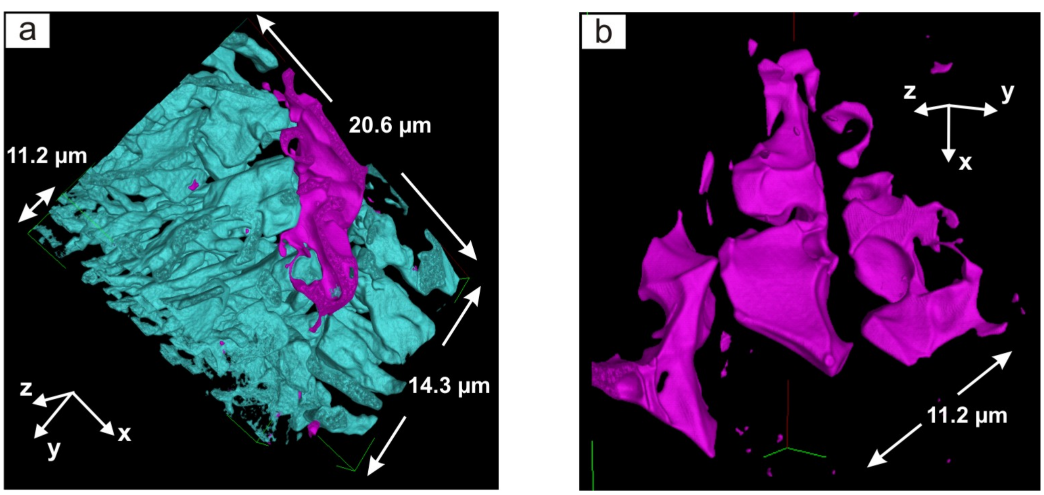

Figure 5: FIB tomography of Sr-modified Al-10Si alloy: (a) 3D morphology of eutectic Si (in cyan) and Fe-rich α-phase (in magenta) observed in region 2 of Fig. 2(b). (b) Fe-rich α-phase visualized without the adjacent eutectic Si.

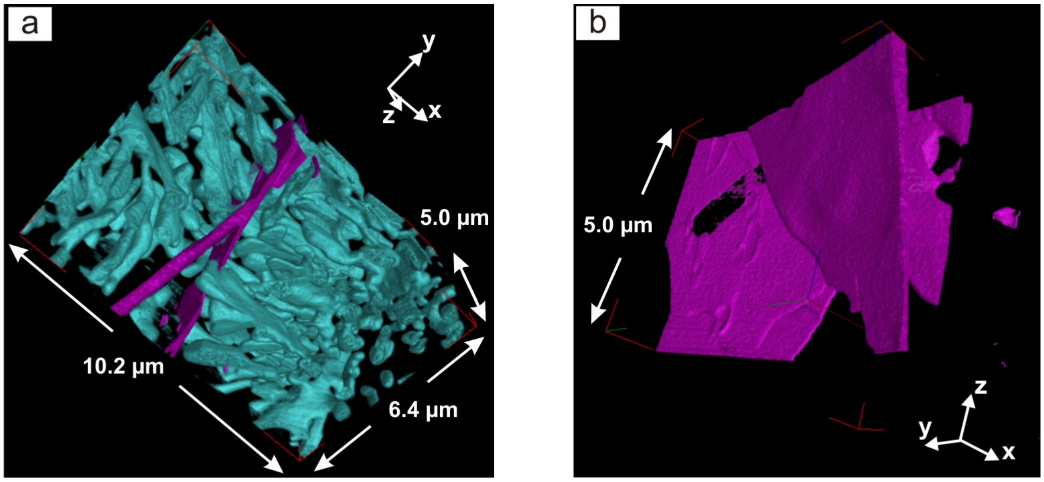

Figure 6: FIB tomography of Sr-modified Al-10Si alloy: (a) 3D morphology of eutectic Si (in cyan) and Fe-rich δ-platelets (in magenta) observed in region 3 of Fig. 2(b). (b) Fe-rich δ-platelets visualized without the adjacent eutectic Si.

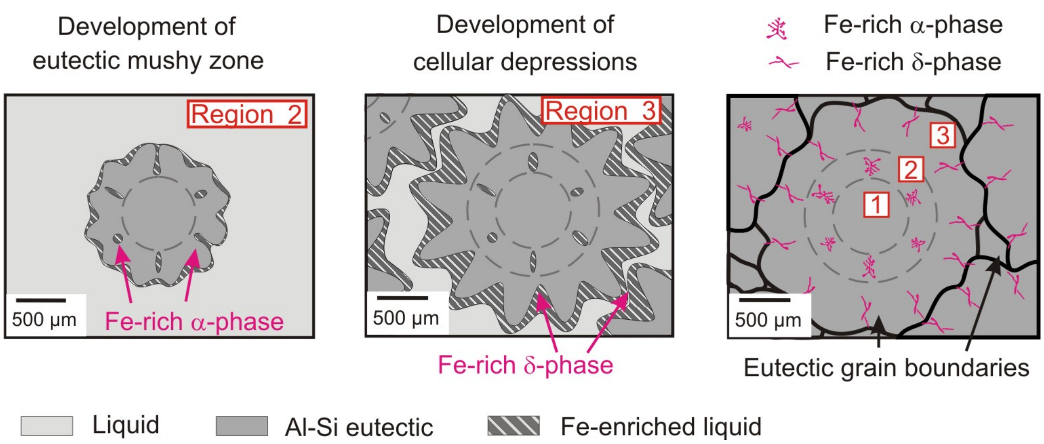

Figure 7: (a) Schematical illustration of the morphological evolution of eutectic growth interface as well as location of both Fe-rich phases in the eutectic grains in Sr-modified alloys containing further impurities such as Fe. Primary Al dendrites are not shown for clarity. (a) Region 2; (b) region 3; (c) solidified eutectic grains structure.